Response of a Memristive Biomembrane and Demonstration of Potential Use in Online Learning

Md Sakib Hasan, Joseph S. Najem, Ryan Weiss, Catherine D. Schuman, Alex Belianinov, C. Patrick Collier, Stephen A. Sarles, and Garrett S. Rose

The online home for this paper may be found at: http://web.eecs.utk.edu/ grose4/

Citation Information (BibTex):

```
@INPROCEEDINGS{hasan2018response,
  author=" Md Sakib Hasan and Joseph S. Najem and Ryan Weiss
and Catherine D. Schuman and Alex Belianinov and C. Patrick
Collier and Stephen A. Sarles and Garrett S. Rose",
  title="Response of a Memristive Biomembrane and
Demonstration of Potential Use in Online Learning",
  booktitle="{IEEE} 13th Nanotechnology Materials and Devices
Conference {NMDC}",
  month="October",
  year="2018",
  pages="1-4",
  address="Portland, OR, USA"
}
```

Response of a Memristive Biomembrane and Demonstration of Potential Use in Online Learning

Md Sakib Hasan*, Joseph S. Najem†‖, Ryan Weiss*, Catherine D. Schuman‡,
Alex Belianinov§, C. Patrick Collier§, Stephen A. Sarles‖, and Garrett S. Rose*

*Department of Electrical Engineering & Computer Science, University of Tennessee, Knoxville, TN 37996 USA
†Joint Institute for Biological Sciences, Oak Ridge National Laboratory, Oak Ridge, TN 37831 USA
‡Computer Science and Mathematics Division, Oak Ridge National Laboratory, Oak Ridge, TN 37831 USA
§Center for Nanophase Materials Sciences, Oak Ridge National Laboratory, Oak Ridge, TN 37831 USA
‖Deparment of Mechanical, Aerospace and Biomedical Engineering, University of Tennessee, Knoxville, TN 37916 USA

Abstract—**The pervasive von Neumann architecture uses complex processor cores and sequential computation. In contrast, the brain is massively parallel and highly efficient, owing to the ability of the neurons and synapses to store and process information simultaneously and to adapt according to incoming information. These features have motivated researchers to develop a host of brain-inspired computers, devices, and models, collectively referred to as neuromorphic computing systems. The quest for synaptic materials capable of closely mimicking biological synapses has led to an alamethicin-doped, synthetic biomembrane with volatile memristive properties which can emulate key synaptic functions to facilitate learning and computation. In contrast to its solid-state counterparts, this two-terminal, biomolecular memristor features similar structure, switching mechanisms, and ionic transport modality as biological synapses while consuming considerably lower power. To use the device as a circuit element, it is important to understand its response to different kinds of input signals. Here we develop a simplified closed form analytical solution based on the underlying state equations for pulse and sine wave inputs. A Verilog-A model based on Runge-Kutta method was developed to incorporate the device in a circuit simulator. Finally, the paper demonstrates possible applications for short- and long-term learning using its unique volatile memristive properties.**

I. Introduction

The imminent demise of Moore's Law and the problem of low bandwidth between CPU and memory (von Neumann bottleneck) has driven researchers to look for alternative computing paradigms. Neuromorphic computing is a computing paradigm inspired by the interconnectivity, performance, and energy efficiency of the brain. The brain uses sophisticated molecular mechanisms to continually reconfigure connectivity between neurons through synaptic plasticity [1] which enables the brain to remember patterns, adapt to incoming information, and perform massive amounts of parallel operations with significantly low levels of power consumption [2]. However, most of the current solid-state devices used for neuromorphic computing do not exhibit biologically realistic structural and functional attributes and, consequently, require far more complex neural networks and power to achieve similar computational capability. A possible alternative approach is to design more biologically faithful systems that are energy-efficient, soft, stochastic, fault-tolerant, and preferably biological. To this end,

a biomolecular memristor (memory resistor) with composition, structure, switching mechanism, and ionic transport similar to biosynapses has been recently reported by Najem et al. [3]. The reversible and volatile voltage-driven insertion of alamethicin peptides into an insulating lipid bilayer creates conductive pathways that exhibit pinched current-voltage hysteresis at potentials above their insertion threshold. This device can emulate key synaptic functions including paired-pulse facilitation (PPF) and depression (PPD) due to a generic memristive property, enabling learning and computation with considerably lower power consumption. Moreover, the synapse-like dynamic properties of the device enables simplified learning circuit implementations.

The remainder of the paper is organized as follows: In Section II, we explore the physical mechanism resulting in volatile memristance and validate the model used to describe the device operation. In Section III, we solve the state equations underlying its memristive charecteristic to derive closed form analytical solution for pulse and sinusoidal inputs. In Section IV, we develop VerilogA model to integrate the device in standard circuit simulator and discuss simulation results from example circuits to show how the unique device functinality can be used to accomplish long-time learning mechanism such as STDP(Spike Time Dependent Plasticity) and short-time learning mechanism such as SRDP(Spike Rate Dependent Plasticity). Finally, we discuss our results and conclude the paper in Section V.

II. Device operation and model validation

The biomolecular memristor consists of an alamethicin-doped synthetic biomembrane of 3-5 nm thickness. The highly insulating ($\sim$10 GΩ) lipid membrane self assembles at the interface of two in-contact, lipid-encased aqueous droplets placed in a reservoir of hexadecane oil. In the presence of alamethicin (alm) peptides (in both droplets) and sufficient transmembrane voltage, conductive ionic pathways are created through volatile, voltage-driven insertion of alm peptides into the insulating lipid membrane. At low voltages, where alm peptides are surface-bound, the device is considered to be in the resting state with very high resistance. However, when the voltage exceeds a threshold potential, the device abruptly switches into a voltage-

dependent conductive state. This mechanism is very similar to the voltage-modulated variable conductance in biosynapses.

The device behavior is governed by two voltage-dependent state variables: the areal density of alamethicin channels N_a, and the increase in membrane area A_m due to electrowetting, which in turn dictates the total number of ion channels, and, thus, the net conductance of the device. Compared to prior memristive devices, this biomolecular memristor consumes significantly less power (0.1-10 nW), is relatively low-cost, and scalable to support large-network computing applications.

The current-voltage relationship of a generic voltage-controlled memristor can be written as

$$I = G(x)V \tag{1}$$

$$\frac{dx}{dt} = f(\mathbf{x}; V) \tag{2}$$

Here, G is the nominal memory conductance and $\mathbf{x}$ represents one or more voltage-controlled state variables that control the conductance [4]. Here, we consider N_a, and A_m, as two state variables for our device.

The insertion of alamethicin peptides and subsequent formation of ion channels (pores) in response to an increase in transmembrane voltage is well characterized [5] [6]. The steady state fractional increase in area through electrowetting caused by applied voltage has also been reported in [7]. For an applied voltage V, the state equations for N_a and A_m, as derived in [3], are

$$\frac{dN_a}{dt} = a_1 + a_2 N_a \tag{3}$$

$$\frac{dA_m}{dt} = b_1 + b_2 A_m \tag{4}$$

where,

$$a_1 = \frac{N_0 exp(|V|/V_e)}{\tau_0 exp(|V|/V_t)}, \quad a_2 = \frac{-1}{\tau_0 exp(|V|/V_t)}$$

$$b_1 = \frac{\alpha V^2}{\tau_{ew}}, \quad b_2 = \frac{-1}{\tau_{ew}}$$

Here, V_e , N_0, V_τ and τ_0 are the voltage required to cause an e-fold increase in the number of alm pore, a proportionality constant that represents the number of alm pores at zero volts, the voltage required to induce an e-fold increase in τ, and the time constant for pore closure at zero volts, respectively. α and τ_{ew} are voltage-sensitivity constant, and characteristic time constant describing electrowetting process, respectively. Combining these results, the overall conductance can be written as,

$$G(t) = G_u N_a(t) A_0 (1 + A_m(t)) \tag{5}$$

where A_0 and G_u are bilayer area at zero volts and average unit conductance of a single alm pore.

τ_{ew} and α were determined by fitting numerical solutions of equation 4 to the measured change in membrane area during voltage sweeps and these, along with measured relaxation time constants (τ_0), were used in another fitting routine to estimate the parameters for alm insertion by fitting numerical solutions

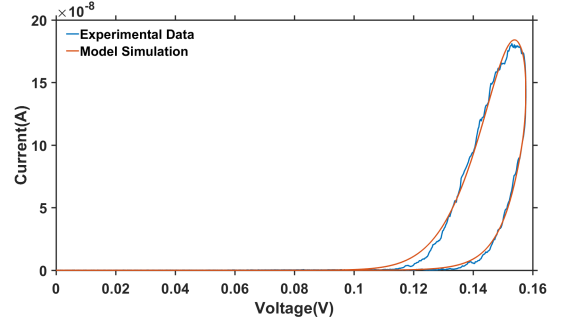

Fig. 1: Comparison between experimental data and model result for pinced hysteresis loop for periodic triangular wave input.

of equation 3 to measured *I-V* responses. These parameters and corresponding conductance can be varied by changing lipid type, alm concentration, temperature etc. The pinched hysteresis *I-V* curve of DPhPC memristor for 0.17 Hz triangular wave of amplitude 160 mV is shown in Fig. 1. The values of the parameters used here are, $V_e = 0.0063\,V$, $V_t = 0.0617\,V$, $N_0 = 0.17$, $\tau_0 = 10\,ms$, $\alpha = 14.4\,V^{-2}$, $\tau_{ew} = 1.5\,s$ and $G_u = 5\,nS$. As seen in this figure, the model fits reasonably well with the measured experimental data.

III. RESPONSE TO PULSE AND SINUSOIDAL INPUT VOLTAGE

A. Pulse Input

For pulse input, coefficients a_1, a_2, b_1 and b_2 will be different from ON to OFF cycle depending on V_{ON} and V_{OFF}. A closed form analytical solution for N_a and A_m can be derived as,

$$N_{ON}^i(t) = (N_{initON}^i + \frac{a_{1ON}}{a_{2ON}}) exp(a_{2ON}t) - \frac{a_{1ON}}{a_{2ON}}$$

$$N_{OFF}^i(t) = (N_{initOFF}^i + \frac{a_{1OFF}}{a_{2OFF}}) exp(a_{2OFF}t) - \frac{a_{1OFF}}{a_{2OFF}}$$

$$A_{ON}^i(t) = (A_{initON}^i + \frac{b_{1ON}}{b_{2ON}}) exp(b_{2ON}t) - \frac{b_{1ON}}{b_{2ON}}$$

$$A_{OFF}^i(t) = (A_{initOFF}^i + \frac{b_{1OFF}}{b_{2OFF}}) exp(b_{2OFF}t) - \frac{b_{1OFF}}{b_{2OFF}}$$

The initial values have to be updated for every cycle to the final value of the previous cycle i.e.

$$N_{initON}^i = N((i-1)T), \quad N_{initOFF}^i = N((i-1)T + T_{ON})$$

$$A_{initON}^i = A((i-1)T), \quad A_{initOFF}^i = A((i-1)T + T_{ON})$$

$$i = number\ of\ cycles, \quad T = T_{ON} + T_{OFF} = Period$$

For a input pulse train with a short off time, more pores will be available for conduction during each subsequent pulse resulting in an increase in average conductance and current. This can be clearly seen in Fig. 2 where the results are plotted based on the above analytical solutions. Here, $T_{ON} = 10\,ms$, $T_{OFF} = 5\,ms$, $V_{ON} = 150\,mV$ and $V_{OFF} = 0\,V$.

B. Sinusoidal input

The response of this device to sinusoidal input requires more involved analysis. For sinusoidal input, $v(t) = O + A\,sin(\omega t)$. Here, $O = Offset, A = amplitude, \omega = angular\ frequency$.
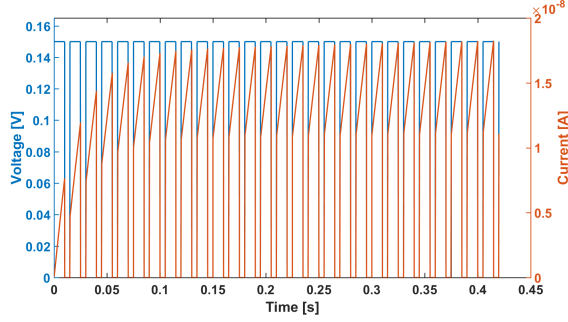
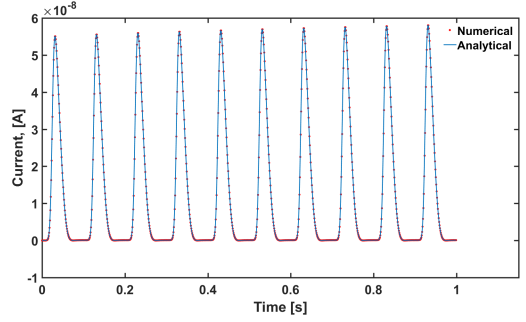Fig. 2: Results from analytical solution for a pulse train input.

Fig. 3: Comparison between numerical simulation and analytical solution of current response for sinusoidal input.

For a first order equation of the form $\frac{dy}{dt} + p(t)y = g(t)$, the general solution is

$$y(t) = \frac{\int \mu(t)g(t)dt + C}{\mu(t)} \qquad (6)$$

Here, $\mu(t) = e^{\int p(t)dt}$. Both the state equations 3 and 4 can be rewritten in this format.

For Pore generation, $p(t) = ce^{dv(t)}$ and $g(t) = ae^{bv(t)}$ where, $a = \frac{N_0}{\tau_0}$, $b = \frac{1}{V_e} - \frac{1}{V_t}$, $c = \frac{1}{\tau_0}$, $d = -\frac{1}{V_t}$.

The solutions of these equations entails expanding periodic functions of the form e^{sinx} and e^{cosx} in fourier series, computing the fourier coefficients using modified Bessel function and truncating the higher harmonic terms of negligible magnitude. The complete derivation is quite long but the final closed form solution can be summarized as,

$$N_a(t) = \frac{Nu(t) + C_1}{\mu(t)} \qquad (7)$$

Here, $Nu(t) \approx \frac{k_3 m_0 e^{k_4 t}}{k_4} + k_3 \sum_{i=1}^{12} P_i^1(t) + k_3 \sum_{i=1}^{11} P_i^2(t)$

$\mu(t) \approx e^{k_2}(a_0^1 \omega t + \sum_{n=1}^{4}[\frac{a_n^1 sin(n\omega t)}{n} - \frac{b_n^1 cos(n\omega t)}{n}])$

$P_i^1(t) = \frac{m_i}{(i\omega)^2 + k_4^2} e^{k_4 t}(i\omega sin(i\omega t) + k_4 cos(i\omega t)); i \in \mathbb{Z}$

$P_i^2(t) = \frac{n_i}{(i\omega)^2 + k_4^2} e^{k_4 t}(k_4 sin(i\omega t) + i\omega cos(i\omega t)); i \in \mathbb{Z}$

$k_1 = ce^{dO}$, $k_2 = \frac{k_1}{\omega}$, $k_3 = ae^{bO}$, $k_4 = k_2 a_0 \omega$, $z_1 = dA$, $z_2 = bA$, $z_3 = -k_2 b_1^1$, $z_4 = \frac{-k_2 b_3^1}{3}$, $a_0^1 = I_0(z_1)$, $a_n^1 = (I_n(z_1) + (-1)^n I_n(z_1))(-1)^{n/2}$, $b_n^1 = (I_n(z_1) + (-1)^{n-1} I_n(z_1))(-1)^{\frac{n-1}{2}}$, $a_0^2 = I_0(z_2)$, $a_n^2 = (I_n(z_2) + (-1)^n I_n(z_2))(-1)^{n/2}$, $b_n^2 = (I_n(z_2) + (-1)^{n-1} I_n(z_2))(-1)^{\frac{n-1}{2}}$, $a_0^3 = I_0(z_3)$, $a_n^3 = 2I_n(z_3)$, $b_n^3 = 0$, $a_0^4 = I_0(z_4)$, $a_n^4 = 2I_n(z_4)$, $b_n^4 = 0$, $I_n(z) = $ modified bessel function of the first kind of order n.

$m_0 = g_1 + \frac{g_{24}}{2}$, $m_1 = g_{12} + \frac{g_{13}}{2}$, $m_2 = g_2 + g_{23} + g_{25}/2$, $m_3 = g_{13}/2 + g_{14}/2$, $m_4 = g_3 + g_{24}/2 + g_{26}/2$, $m_5 = g_{14}/2 + g_{15}/2$, $m_6 = g_4 + g_{25}/2 + g_{27}/2$, $m_7 = g_{15}/2 + g_{16}/2$, $m_8 = g_5 + g_{26}/2 + g_{28}/2$, $m_9 = g_{16}/2 + g_{17}/2$, $m_{10} = g_6 + g_{27}/2$, $m_{11} = g_{17}/2$, $m_{12} = g_{28}/2$, $m_{13} = g_{29}/2$, $m_{14} = g_7 + g_{30}/2$, $m_{15} = g_{18}/2 + g_{19}/2$, $m_{16} = g_8 + g_{29}/2 + g_{31}/2$, $m_{17} = g_{19}/2 + g_{20}/2$, $m_{18} = g_9 + g_{30}/2 + g_{32}/2$, $m_{19} = g_{20}/2 + g_{21}/2$, $m_{20} = g_{10} + g_{31}/2 + g_{33}/2$, $m_{21} = g_{21}/2 + g_{22}/2$, $m_{22} = g_{11} + g_{32}/2$, $m_{23} = g_{22}/2$, $m_{24} = g_{33}/2$.

$$g_i = \begin{cases} q_0 a_{2i-2}^2 & 1 \le i \le 6 \\ q_0 b_{2i-13}^2 & 7 \le i \le 11 \\ q_1 a_{2i-24}^2 & 12 \le i \le 17 \\ q_1 b_{2i-35}^2 & 18 \le i \le 22 \\ q_2 a_{2i-46}^2 & 23 \le i \le 28 \\ q_2 b_{2i-57}^2 & 29 \le i \le 33 \end{cases}$$

$q_i = a_0^4 a_i^3; 0 \le i \le 2$

$$n_i = \begin{cases} m_{14} - m_{13} & i = 1 \\ m_{i+13} & 2 \le i \le 11 \end{cases}$$

The constant C_1 can be determined from initial condition as $C_1 = N_a(0)\mu(0) - Nu(0)$.

For electrowetting, $p(t) = \frac{1}{\tau_{EW}}$, $g(t) = \frac{\alpha v^2}{\tau_{EW}}$.

$$A_m(t) = \frac{\int e^{a_2 t} \alpha v^2(t)dt + C_2}{\mu(t)}$$
$$= \frac{\alpha a_2 [A_1(t) + A_2(t) + A_3(t) - A_4(t)] + C_2}{e^{a_2 t}} \qquad (8)$$

$A_1(t) = \frac{O^2 e^{a_2 t}}{a_2}$, $A_2(t) = \frac{2OA e^{a_2 t}(a_2 sin(\omega t) - \omega cos(\omega t))}{a_2^2 + \omega^2}$,

$A_3(t) = \frac{A^2 e^{a_2 t}}{2a_2}$, $A_4(t) = \frac{A^2 e^{a_2 t}(2\omega sin(2\omega t) + a_2 cos(2\omega t))}{2(a^2 + 4\omega^2)}$.

C_2 can be determined using the initial condition. For $A_m(0) = 0$, we get, $C_2 = -\alpha a[\frac{O^2}{a_2} + \frac{-2OA\omega}{a_2^2 + \omega^2} + \frac{A^2}{2a_2} - \frac{a_2 A^2}{2(a_2^2 + 4\omega^2)}]$.

Since some approximations were used to arrive at these results, the validity of the final solution is validated against numerical simulation for sine wave as shown in Fig. 3. Here, $O = A = 75mV$, $\omega = 62.83\,rads^{-1}$.

IV. IMPLEMENTATION IN CIRCUIT SIMULATOR AND LEARNING APPLICATIONS

The model was also implemented in VerilogA and simulated using Cadence Spectre circuit simulator. For the VerilogA implementation, the state equations were solved numerically using fourth order Runge-Kutta method. Here, each value of N_a and A_m is computed iteratively. First, we assume $\frac{dN_a}{dt} = f(N_a)$, $\frac{dA_m}{dt} = f(A_m)$ and the value of N_a and A_m at n^{th} iteration is N_a^n and A_m^n. Then, in each iteration, we define

$k_1 = f(N_a^n), k_2 = f(N_a^n + k_1/2), k_3 = f(N_a^n + k_2/2), k_4 = f(N_a^n + k_3)$ and $q_1 = f(A_m^n), q_2 = f(A_m^n + k_1/2), q_3 = f(A_m^n + k_2/2), q_4 = f(A_m^n + k_3)$. The value of state variables in the next iteration will be, $N_a^{n+1} = N_a^n + \frac{1}{6}(k_1 + 2k_2 + 2k_3 + k_4)$ $A_m^{n+1} = A_m^n + \frac{1}{6}(q_1 + 2q_2 + 2q_3 + q_4)$. Once, the state variables are calculated, eqn 1 and eqn 5 are used to calculate the response current.

As evident from Fig. 2, this biomolecular device offers opportunity for learning mechanisms like SRDP which plays an important role in synaptic computations [8]. It is shown in Fig. 4 by plotting the relative change is average device resistance for two successive pulses with varying OFF time. Here, different pulse parameters such as OFF voltage and ON time are varied to show their effect on the amount of PPF.
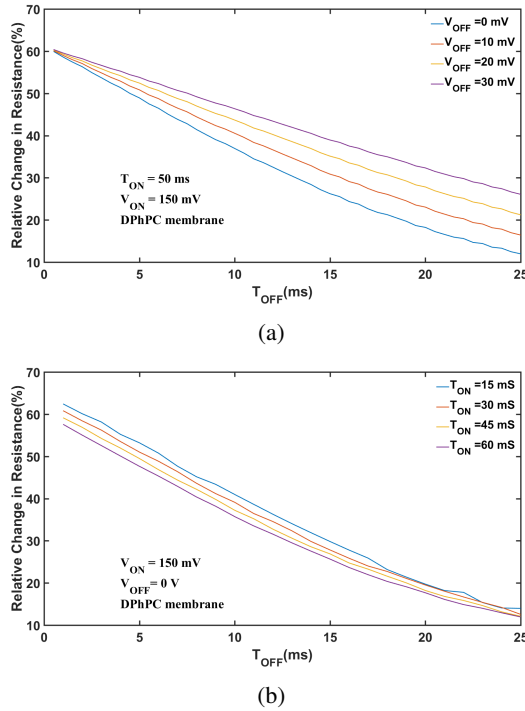

(a)

(b)

Fig. 4: Effect of pulse parameters on SRDP, (a) varying OFF voltage, b) varying ON time.
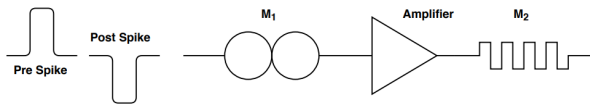

Fig. 5: Simplified schematic of a circuit containing Non-volatile and bio-memristor to implement STDP.

The PPF property of the device can also be used to facilitate long time learning mechanism such as STDP. A simplified schematic of an example circuit is shown in Fig. 5, where a non volatile memristor(M_2) is used as synaptic weight and is
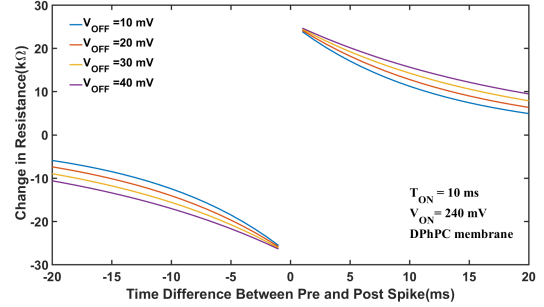

Fig. 6: Effect of pulse parameter on STDP

updated based on the time difference between pre and post spike. This synaptic update is accomplished using a our bio-memristor(M_1) along with a trans-impedance amplifier. The results for different OFF voltages are shown in Fig. 6.

V. Conclusion

This paper describes a soft matter memristor capable of emulating biologically realistic synaptic plasticity and presents analytical solution of the response current for pulse and si-nusoidal input. We have also developed a Verilog-A model to integrate the device as a circuit element in circuit simulator and simulated example circuits to demonstrate potential application in online learning. As shown in this paper, the unique capability of this device will enable more biologically realistic next generation spiking neural network hardware.

Acknowledgment

References

[1] M. Mayford, S. A. Siegelbaum, and E. R. Kandel, "Synapses and memory storage," *Cold Spring Harbor perspectives in biology*, vol. 4, no. 6, p. a005751, 2012.

[2] M. P. van den Heuvel, C. J. Stam, R. S. Kahn, and H. E. H. Pol, "Efficiency of functional brain networks and intellectual performance," *Journal of Neuroscience*, vol. 29, no. 23, pp. 7619–7624, 2009.

[3] J. S. Najem, G. J. Taylor, R. J. Weiss, M. S. Hasan, G. Rose, C. D. Schuman, A. Belianinov, C. P. Collier, and S. A. Sarles, "Memristive ion channel-doped biomembranes as synaptic mimics," *ACS Nano*, vol. 12, no. 5, pp. 4702–4711, mar 2018.

[4] C. Leon, "Everything you wish to know about memristors but are afraid to ask," *Radioengineering*, vol. 24, no. 2, p. 319, 2015.

[5] M. Eisenberg, J. E. Hall, and C. Mead, "The nature of the voltage-dependent conductance induced by alamethicin in black lipid membranes," *The Journal of membrane biology*, vol. 14, no. 1, pp. 143–176, 1973.

[6] T. Okazaki, M. Sakoh, Y. Nagaoka, and K. Asami, "Ion channels of alamethicin dimer n-terminally linked by disulfide bond," *Biophysical journal*, vol. 85, no. 1, pp. 267–273, 2003.

[7] G. J. Taylor, G. A. Venkatesan, C. P. Collier, and S. A. Sarles, "Direct in situ measurement of specific capacitance, monolayer tension, and bilayer tension in a droplet interface bilayer," *Soft matter*, vol. 11, no. 38, pp. 7592–7605, 2015.

[8] P.-Y. Deng and V. A. Klyachko, "The diverse functions of short-term plasticity components in synaptic computations," *Communicative & integrative biology*, vol. 4, no. 5, pp. 543–548, 2011.